Construction of complex Co3O4@Co3V2O8 hollow structures from metal-organic frameworks with enhanced lithium storage properties

Lu, Yan; Yu, Le; Wu, Minghong; Wang, Yong; Lou, David Xiong Wen

2018

Lu, Y., Yu, L., Wu, M., Wang, Y., & Lou, D. X. W. (2018). Construction of complex Co3O4@Co3V2O8 hollow structures from metal-organic frameworks with enhanced lithium storage properties. Advanced materials, 30(1), 1702875-. doi:10.1002/adma.201702875

https://hdl.handle.net/10356/138672

https://doi.org/10.1002/adma.201702875

Construction of Complex Co_3O_4@$Co_3V_2O_8$ Hollow Structures from Metal-Organic Frameworks with Enhanced Lithium Storage Properties

Yan Lu, Le Yu, Minghong Wu, Yong Wang and Xiong Wen (David) Lou[*]

[*] Dr. Y. Lu, Dr. L. Yu, Prof. X. W. Lou

School of Chemical and Biomedical Engineering, Nanyang Technological University, 62 Nanyang Drive, Singapore 637459, Singapore

Email: xwlou@ntu.edu.sg; davidlou88@gmail.com

Webpage: http://www.ntu.edu.sg/home/xwlou/

Prof. M. H. Wu, Prof. Y. Wang

Department of Chemical Engineering, School of Environmental and Chemical Engineering

Shanghai University, 99 Shangda Road, Shanghai 200444, P. R. China

Abstract

We demonstrate a novel metal-organic framework (MOF) engaged strategy for the preparation of multi-shelled Co_3O_4@$Co_3V_2O_8$ hybrid nanoboxes. This strategy relies on the unique reaction of zeolitic imidazolate framework (ZIF)-67 with the vanadium source of vanadium oxytriisopropoxide (VOT). Benefitting from the synthetic versatility, a series of nanostructures can be realized including triple-shelled and double-shelled Co_3O_4@$Co_3V_2O_8$ nanoboxes and single-shelled $Co_3V_2O_8$ nanoboxes. When evaluated as electrode materials for lithium-ion batteries, these unique hollow structures demonstrate remarkable lithium storage properties. For example, the triple-shelled Co_3O_4@$Co_3V_2O_8$ nanoboxes retain a high capacity of 948 mAh g^{-1} after 100 cycles at 100 mA g^{-1}.

Key words: Co_3O_4, $Co_3V_2O_8$, multi-shelled, nanoboxes, lithium-ion batteries

Lithium-ion batteries (LIBs) have taken a large and increasing share of the rechargeable-battery market owing to their excellent performance in terms of cycle life and energy density.[1-3] However, the dominant commercially used anode material, graphite, has a limited theoretical capacity of around 372 mAh g^{-1}, which can hardly meet the ever-growing energy demand for various consumer electronic devices.[4] Recently, considerable effort has been focused on searching for alternative electrode materials that can provide higher capacity and better rate capability.[5,6] Transition metal oxides (TMOs) have been considered as promising anode materials in view of their relatively low cost, environmental benignity, higher theoretical capacity and intrinsically enhanced safety.[7,8] However, their practical application is still hindered by the low intrinsic conductivity and the serious pulverization issue during the lithium insertion and extraction process. As a result, these electrodes usually suffer from poor rate performance and rapid capacity fading in the cycling process. Among these TMOs materials, cobalt oxide (Co_3O_4) can theoretically deliver a specific capacity of 890 mAh g^{-1} due to its 8-electron transfer reaction upon cycling.[9,10] When coupling with vanadium element to form cobalt vanadates (such as $Co_3V_2O_8$), the electrochemical performance of these ternary TMOs can be largely improved owing to the synergistic effect of the two components with enhanced electrical/ionic conductivity, reversible capacity and mechanical stability.[11-13]

It is also noted that hollow structuring of the electrode materials has been proved as a promising avenue to boost the electrochemical performance by effectively alleviating the stress-induced structural variation during long-term electrochemical reactions. Particularly, multi-shelled hollow structures have stimulated tremendous research interest because of their structural advantages with improved weight fraction of active species, complex inner voids, larger surface area and tunable shell compositions compared with the single-shelled hollow structures.[14,15] Although some successful

attempts have been made, most of the obtained multi-shelled hollow structures are in spherical morphologies with relatively simple composition.[9,16-18] It is thus highly desirable yet challenging to tune the compositions within the different shells of multi-shelled hollow structures as hybrid electrode materials for LIBs.

Herein, we demonstrate a novel approach for the effective synthesis of multi-shelled nanoboxes (NBs) of Co_3O_4@$Co_3V_2O_8$ hybrid materials by taking advantage of the unique reactivity of zeolitic imidazolate framework (ZIF)-67 with the vanadium source of vanadium oxytriisopropoxide (VOT). This strategy involves the initial formation of ZIF-67@amorphous-$Co_3V_2O_8$ (ZIF-67@a-$Co_3V_2O_8$) yolk-shelled structures and subsequent thermal annealing in air. The shell number and composition can be precisely controlled by simply tuning the amount of VOT used in the reaction systems, thus allowing the preparation of triple-shelled Co_3O_4@$Co_3V_2O_8$ nanoboxes (T-Co_3O_4@$Co_3V_2O_8$), double-shelled Co_3O_4@$Co_3V_2O_8$ nanoboxes (D-Co_3O_4@$Co_3V_2O_8$) and single-shelled $Co_3V_2O_8$ nanoboxes (S-$Co_3V_2O_8$). We further evaluate the electrochemical performance of the obtained samples as anodes in LIBs. The Co_3O_4@$Co_3V_2O_8$ NBs with the triple-shelled structure manifest the best electrochemical performance compared with the other samples, which shows the advantages of the unique shell architectures and complex compositions.

The synthesis strategy is schematically illustrated in **Figure 1**. First, highly uniform ZIF-67 nanocubes (Figure S1, see Supporting Information) are easily prepared by a modified method.[19] These ZIF-67 nanocubes are dispersed in absolute ethanol solution containing certain amount of VOT and continuously stirred for 20 min to form a clear purple solution. For the typical synthesis of T-Co_3O_4@$Co_3V_2O_8$ NBs, a ZIF-67@a-$Co_3V_2O_8$ yolk-shell structured precursor is first obtained after a solvothermal treatment of the aforementioned solution with the VOT concentration of 50 μL as shown

in step 1. During which, vanadate anion (VO_4^{3-}) generated from VOT is considered to replace the 2-methylimidazole anion gradually in ZIF-67 by ion-exchange to form a-$Co_3V_2O_8$ shell. Meanwhile, the continuous consumption of ZIF-67 core results in a gap space between the newly formed a-$Co_3V_2O_8$ shell and the remaining core. Afterwards, a thermal calcination in air is applied to convert a-$Co_3V_2O_8$ shell and the ZIF-67 core into $Co_3V_2O_8$ and Co_3O_4, respectively. As such, T-Co_3O_4@$Co_3V_2O_8$ NBs can be eventually obtained (Step 2). By precisely tuning the VOT concentration, two other hollow nanostructures of D-Co_3O_4@$Co_3V_2O_8$ and S-$Co_3V_2O_8$ NBs can also be synthesized.

After treated with 50 μL of VOT at 120 ºC for 2 h, the particles (denoted as ZIF-67@a-$Co_3V_2O_8$-50) still retain a cubic shape with high uniformity but bulged in edges (Figure S2A,B, see Supporting Information). Transmission electron microscope (TEM) observations reveal the yolk-shelled features of the transformed sample (Figure S2C, see Supporting Information). It can be seen that the shell is composed of nanoparticles and the shape of the solid core remains cubic. The weak peaks of X-ray diffraction (XRD) pattern for the as-prepared sample can still be ascribed to ZIF-67, indicating the amorphous nature of the shell (Figure S2D, see Supporting Information). Thermal annealing of the ZIF-67@a-$Co_3V_2O_8$-50 sample in air can result in the formation of T-Co_3O_4@$Co_3V_2O_8$ NBs. XRD pattern for the prepared T-Co_3O_4@$Co_3V_2O_8$ sample is first examined (Figure S3A, see Supporting Information). Well-defined peaks ascribed to $Co_3V_2O_8$ (JCPDS card No.: 74-1486) and Co_3O_4 (JCPDS card No.: 74-2120) can be identified, implying the crystallization of the amorphous $Co_3V_2O_8$ shell and the transformation of ZIF-67 core into Co_3O_4. Field-emission scanning electron microscope (FESEM) images (**Figure 2**A; Figure S3B, see Supporting Information) reveal that this sample consists entirely of uniform cubic particles without aggregation even after high temperature annealing.

Furthermore, the TEM image (Figure 2B) clearly shows that the as-synthesized T-Co_3O_4@$Co_3V_2O_8$ NBs possess a triple-shelled structure. The magnified TEM image (Figure 2C) shows the porous feature of these cubic nanocages, which are composed of numerous small nanoparticles. High-resolution TEM (HRTEM) image (Figure 2D) of the outer shell reveals lattice fringes with a *d*-spacing of 0.301 nm, which corresponds to the (002) plane of $Co_3V_2O_8$.

To reveal the spatial distribution of different elements in the T-Co_3O_4@$Co_3V_2O_8$ NBs, elemental mapping analysis is carried out on a representative T-Co_3O_4@$Co_3V_2O_8$ nanobox under scanning transmission electron microscope (STEM) mode. From the high-angle annular dark-field (HAADF)-STEM image (**Figure 3**A), three different shells of the nanobox can be easily identified. The elemental mapping result for Co element (Figure 3B) indicates its uniform distribution within all these three shells. Whereas, the signal intensity of V element (Figure 3C) can be only observed in the outermost shell of the triple-shelled structure. Meanwhile, the O element (Figure 3D) is nearly distributed evenly throughout the structure. Based on the above observations, one can deduce that the T-Co_3O_4@$Co_3V_2O_8$ nanobox has a $Co_3V_2O_8$ outermost shell and two Co_3O_4 inner shells. Furthermore, the distribution of three elements in different shells can be clearly observed from the superimposed mapping result (Figure 3E). The energy-dispersive X-ray (EDX) spectrum reveals that the obtained sample possesses a Co/V atomic ratio of 1.8:1 (Figure S4, see Supporting Information).

To obtain further insight into the formation process of multi-shelled Co_3O_4@$Co_3V_2O_8$ nanoboxes, syntheses with different VOT concentrations are carried out. Without the addition of VOT in the reaction system, the obtained sample remains the solid nature after the reaction (**Figure 4**A). Only some slight corrosions can be found around the surfaces and edges (Figure S5A-C, see Supporting Information). XRD analysis shows these solid particles are still ZIF-67 with good crystallinity (Figure

S5D, see Supporting Information). With the increase of VOT concentration in the reaction system, a variety of hollow nanostructures from yolk-shelled structures to nanoboxes could be obtained. Particularly, at a VOT amount of 50 μL, a thin a-$Co_3V_2O_8$ shell and a large ZIF-67 core are obtained as the yolk-shelled ZIF-67@a-$Co_3V_2O_8$-50 (Figure 4B; Figure S2C, see Supporting Information). When the VOT amount increases to 70 μL, there are no obvious changes for the surface of the ZIF-67@a-$Co_3V_2O_8$-70 cubes (Figure S6A,B, see Supporting Information) compared with the ZIF-67@a-$Co_3V_2O_8$-50 sample. TEM observations reveal a similar yolk-shelled structure for ZIF-67@a-$Co_3V_2O_8$-70 with a thicker a-$Co_3V_2O_8$ shell and a shrunken ZIF-67 core (Figure 4C; Figure S6C, see Supporting Information). With the further increase of VOT amount to 120 μL, the obtained sample has a rather rough surface, which is assembled by nanoparticles with larger size (Figure S6D,E, see Supporting Information). Furthermore, TEM investigations indicate the ZIF-67 core is completely consumed to generate single-shelled a-$Co_3V_2O_8$ nanoboxes (Figure 4D; Figure S6F, see Supporting Information).

Afterwards, the as-synthesized particles are annealed in air to obtain a variety of hollow structures. The sample treated without VOT (Figure 4A) is converted into Co_3O_4 nanocubes with a porous structure as shown in Figure 4E,I. Due to the strong structural stress during the thermal treatment, the obtained Co_3O_4 particles exhibit concave surfaces with negative curvature (Figure S7A,B, see Supporting Information).[10,20] Meanwhile, triple-shelled (Figure 4F,J), double-shelled (Figure 4G,K; Figure S7D,E, see Supporting Information) Co_3O_4@$Co_3V_2O_8$ and single-shelled $Co_3V_2O_8$ (Figure 4H,L; Figure S7G,H, see Supporting Information) structures are obtained after thermal treatments, which are derived from the yolk-shelled ZIF-67@a-$Co_3V_2O_8$-50, ZIF-67@a-$Co_3V_2O_8$-70 and single-shelled a-$Co_3V_2O_8$ nanoboxes, respectively. XRD pattern for the obtained Co_3O_4 nanocubes confirms

its Co_3O_4 phase without any impurity (Figure S7C, see Supporting Information). Meanwhile, XRD pattern (Figure S7F, see Supporting Information) and element mapping results (Figure S8, see Supporting Information) reveal the presence and spatial distribution of $Co_3V_2O_8$ and Co_3O_4 in the prepared D-Co_3O_4@$Co_3V_2O_8$ NBs. For the S-$Co_3V_2O_8$ NBs, only the $Co_3V_2O_8$ phase is detected from the XRD data (Figure S7I, see Supporting Information) with Co, V and O homogeneously distributed in the shell (Figure S9, see Supporting Information). The N_2 sorption measurements reveal that T-Co_3O_4@$Co_3V_2O_8$ NBs possess a larger Brunauer-Emmett-Teller (BET) specific surface area of 77 m^2 g^{-1} compared with D-Co_3O_4@$Co_3V_2O_8$ NBs (59 m^2 g^{-1}) and S-$Co_3V_2O_8$ NBs (46 m^2 g^{-1}), showing the advantages of the multi-shelled hollow structure (Figure S10, see Supporting Information). Meanwhile, the pore size distribution curves indicate that these three samples have a relatively narrow pore size distribution in the range of 2~12 nm. Compared with the reported synthesis approaches for multi-shelled structures, such as sequential templating approach,[15,21] carbonaceous microspheres templated method,[9,17,22] and programmable heating method,[18,23] the present strategy not only opens a new avenue for the synthesis of non-spherical multi-shelled hollow structures but also provides the possibility to manipulate the shell compositions.

We next evaluate the electrochemical lithium storage properties of these samples for their potential use as anode materials for LIBs. **Figure 5**A shows representative discharge/charge voltage profiles of T-Co_3O_4@$Co_3V_2O_8$ NBs at a current density of 100 mA g^{-1} within a cut-off voltage window of 0.01-2.5 V. In the first discharge curve, two pronounced plateaus around 0.8 V and 0.2 V are observed, which might be associated with the complex transformations of Co_3O_4 and $Co_3V_2O_8$ to Co^0 and $Li_xV_2O_5$ upon lithiation reaction as well as the possible irreversible formation of solid electrolyte interface.[11,12,24-26] The representative cyclic voltammetry (CV) curves of the T-Co_3O_4@$Co_3V_2O_8$

electrode are in good agreement with the discharge-charge voltage profiles, further confirming the typical electrochemical processes of the hybrid material (Figure S11, see Supporting Information). The T-Co_3O_4@$Co_3V_2O_8$ NBs deliver an initial discharge capacity of 1909 mAh g^{-1} and a reversible charge capacity of 1186 mAh g^{-1} in the first cycle, indicating the highest initial Coulombic efficiency (CE) of 62% among all the electrodes (Figure S12A, see Supporting Information). It is noteworthy that the voltage profile of the 50th-cycle discharge curve is different from the second-cycle discharge curve. The signal washout with the increased cycle number might be attributed to continuous pulverization of the electrode materials from nanoparticles into numerous quantum dots during the repeated lithiation processes.[11,27]

The high-rate capability of electrode materials is of great importance for the potential high-power applications. As evaluated by galvanostatic measurements at various current densities, the T-Co_3O_4@$Co_3V_2O_8$ electrode exhibits enhanced rate performance with average specific capacities of 1068, 916, 782, 678, 578 and 550 mAh g^{-1} at current densities of 100, 200, 500, 1000, 2000 and 5000 mA g^{-1}, respectively (Figure 5B). Moreover, a stable capacity of about 902 mAh g^{-1} can be delivered when the current density is reduced back to 100 mA g^{-1}, indicating its good reversibility. Of note, T-Co_3O_4@$Co_3V_2O_8$ NBs also possesses better rate capability in terms of better cycling stability and higher capacity at each current rate compared with control samples (Figure S12B, see Supporting Information).

The cycling performance and the corresponding Coulombic efficiency of the T-Co_3O_4@$Co_3V_2O_8$ NBs is presented in Figure 5C. At a current density of 100 mA g^{-1}, the specific capacity quickly stabilizes at 1062 mAh g^{-1} after the gradual capacity decay in the first 10 cycles. A reversible capacity of 948 mAh g^{-1} can still be retained over 100 cycles with a high CE of around 97% throughout the

cycling except for the first few cycles, suggesting the impressive cycling stability of T-Co_3O_4@$Co_3V_2O_8$ electrode. Meanwhile, the other samples also show decent cycling performance with relatively lower capacity (Figure S12C, see Supporting Information). The post-mortem study confirms that the overall cubic structure of the T-Co_3O_4@$Co_3V_2O_8$ NBs can be well maintained even after the long-time discharge-charge cycles. This observation suggests that the complex triple-shelled structure could efficiently address the volume expansion during repeated lithium uptake/release processes (Figure S13, see Supporting Information). Even at a much higher current density of 1000 mA g^{-1}, the T-Co_3O_4@$Co_3V_2O_8$ electrode still shows very good cycling stability delivering a capacity as high as 706 mAh g^{-1} after 500 cycles (Figure S14, see Supporting Information).

Notably, the lithium storage properties of T-Co_3O_4@$Co_3V_2O_8$ NBs are superior to those of many other reported Co/V-based oxides (Table S1, see Supporting Information), highlighting their potentials as an anode material in LIBs. Overall, these excellent lithium storage properties demonstrate the structural and compositional advantages of the T-Co_3O_4@$Co_3V_2O_8$ nanoboxes, which might be benefitted from the following aspects. First, the reduced particle size of the electroactive materials would not only shorten the electronic/ionic pathways for the high rate lithium insertion/removal, but also accommodate the strain of the volume change during lithium storage process.[28,29] Second, the unique multi-shelled structures can effectively prevent the agglomeration of the nanoparticles to expose more active sites during the repeated lithium insertion/extraction processes. In addition, the confinement of the electrolyte between the shells further guarantees the intimate contact of the active materials with the electrolyte for the enhanced capacity and rate performance.[30] Furthermore, the complex hollow structures with high weight fraction of active species is beneficial for improved volumetric energy density and power density.[14] Compared with

single-shelled and double-shelled counterparts, the triple-shelled sample with a larger surface area might provide more electroactive sites for higher specific capacity. Most importantly, superior to single-component electrode materials, the hybridization of two electrochemically active components in such a complex nanostructure might gain extra benefits in terms of the enhanced mechanical stability, electrical/ionic conductivity, reversible capacity, and mechanical stability.

In summary, unique multi-shelled Co_3O_4@$Co_3V_2O_8$ hybrid nanoboxes have been successfully prepared. The synthesis involves the unique reaction between zeolitic imidazolate framework (ZIF)-67 particles with vanadium oxytriisopropoxide (VOT) under solvothermal conditions followed by thermal annealing in air. By simply tuning the VOT concentrations in the reaction, a series of nanostructures can be readily obtained from single-shelled $Co_3V_2O_8$ nanoboxes to double-shelled and triple-shelled Co_3O_4@$Co_3V_2O_8$ composite nanoboxes. The triple-shelled Co_3O_4@$Co_3V_2O_8$ nanoboxes exhibit superior lithium storage properties with excellent capacity performance, cycling stability and rate performance. This work may open a new avenue for the design and synthesis of complex hollow structures with tailorable structure and composition for a variety of applications.

Acknowledgements

X. W. L. acknowledges the funding support from the National Research Foundation (NRF) of Singapore via the NRF Investigatorship (NRF-NRFI2016-04).

References

[1] M. Armand, J. M. Tarascon, *Nature* **2008**, *451*, 652.

[2] B. Scrosati, J. Hassoun, Y. K. Sun, *Energy Environ. Sci.* **2011**, *4*, 3287.

[3] B. Dunn, H. Kamath, J. M. Tarascon, *Science* **2011**, *334*, 928.

[4] F. Zou, X. Hu, Z. Li, L. Qie, C. Hu, R. Zeng, Y. Jiang, Y. Huang, *Adv. Mater.* **2014**, *26*, 6622.

[5] V. Etacheri, R. Marom, R. Elazari, G. Salitra, D. Aurbach, *Energy Environ. Sci.* **2011**, *4*, 3243.

[6] C. Liu, F. Li, L. P. Ma, H. M. Cheng, *Adv. Mater.* **2010**, *22*, E28.

[7] C. Yuan, H. B. Wu, Y. Xie, X. W. Lou, *Angew. Chem. Int. Ed.* **2014**, *53*, 1488.

[8] M. Reddy, G. Subba Rao, B. Chowdari, *Chem. Rev.* **2013**, *113*, 5364.

[9] J. Wang, N. Yang, H. Tang, Z. Dong, Q. Jin, M. Yang, D. Kisailus, H. Zhao, Z. Tang, D. Wang, *Angew. Chem. Int. Ed.* **2013**, *125*, 6545.

[10] J. Shao, Z. Wan, H. Liu, H. Zheng, T. Gao, M. Shen, Q. Qu, H. Zheng, *J. Mater. Chem. A* **2014**, *2*, 12194.

[11] G. Yang, H. Cui, G. Yang, C. Wang, *ACS Nano* **2014**, *8*, 4474.

[12] Y. Luo, X. Xu, X. Tian, Q. Wei, M. Yan, K. Zhao, X. Xu, L. Mai, *J. Mater. Chem. A* **2016**, *4*, 5075.

[13] F. Wu, S. Xiong, Y. Qian, S. H. Yu, *Angew. Chem. Int. Ed.* **2015**, *54*, 10787.

[14] L. Yu, H. Hu, H. B. Wu, X. W. Lou, *Adv. Mater.* **2017**, *29*, 1604563.

[15] Y. Wang, L. Yu, X. W. Lou, *Angew. Chem. Int. Ed.* **2016**, *128*, 14888.

[16] H. Xu, W. Wang, *Angew. Chem., Int. Ed.* **2007**, *46*, 1489.

[17] S. Xu, C. M. Hessel, H. Ren, R. Yu, Q. Jin, M. Yang, H. Zhao, D. Wang, *Energy Environ. Sci.* **2014**, *7*, 632.

[18] Z. Dong, X. Lai, J. E. Halpert, N. Yang, L. Yi, J. Zhai, D. Wang, Z. Tang, L. Jiang, *Adv. Mater.* **2012**, *24*, 1046.

[19] H. Hu, B. Y. Guan, X. W. Lou, *Chem* **2016**, *1*, 102.

[20] R. Wu, X. Qian, X. Rui, H. Liu, B. Yadian, K. Zhou, J. Wei, Q. Yan, X. Q. Feng, Y. Long, *Small* **2014**, *10*, 1932.

[21] X. Lai, J. Li, B. A. Korgel, Z. Dong, Z. Li, F. Su, J. Du, D. Wang, *Angew. Chem. Int. Ed.* **2011**, *123*, 2790.

[22] G. Zhang, X. W. Lou, *Angew. Chem. Int. Ed.* **2014**, *53*, 9041.

[23] H. B. Lin, H. B. Rong, W. Z. Huang, Y. H. Liao, L. D. Xing, M. Q. Xu, X. P. Li, W. S. Li, *J. Mater. Chem. A* **2014**, *2*, 14189.

[24] Z. S. Wu, W. Ren, L. Wen, L. Gao, J. Zhao, Z. Chen, G. Zhou, F. Li, H. M. Cheng, *ACS Nano* **2010**, *4*, 3187.

[25] V. Soundharrajan, B. Sambandam, J. Song, S. Kim, J. Jo, S. Kim, S. Lee, V. Mathew, J. Kim, *ACS Appl. Mater. Interfaces* **2016**, *8*, 8546.

[26] J. Xiang, X. Y. Yu, U. Paik, *J. Power Sources* **2016**, *329*, 190.

[27] L. Xu, C. Kim, A. K. Shukla, A. Dong, T. M. Mattox, D. J. Milliron, J. Cabana, *Nano Lett.* **2013**, *13*, 1800.

[28] A. S. Arico, P. Bruce, B. Scrosati, J. M. Tarascon, W. Van Schalkwijk, *Nat. Mater.* **2005**, *4*, 366.

[29] P. G. Bruce, B. Scrosati, J. M. Tarascon, *Angew. Chem. Int. Ed.* **2008**, *47*, 2930.

[30] H. Hu, B. Guan, B. Xia, X. W. Lou, *J. Am. Chem. Soc.* **2015**, *137*, 5590.

Figures and Captions

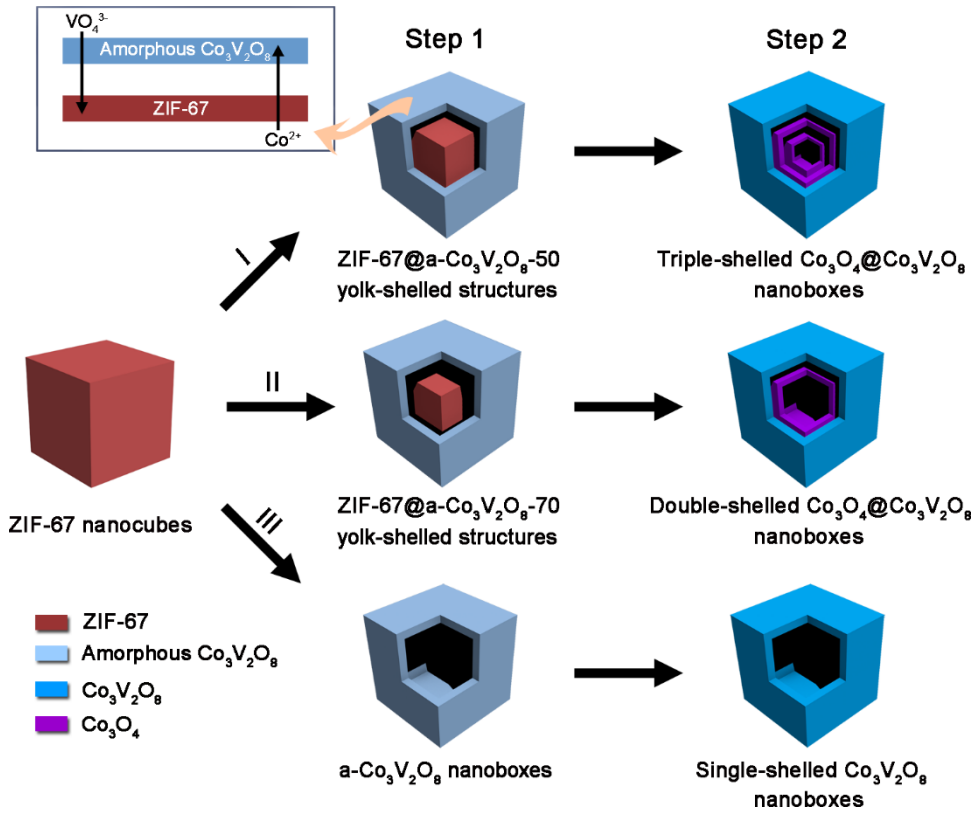

Figure 1. Schematic illustration of the formation of complex Co_3O_4@$Co_3V_2O_8$ hollow structures. The step 1 involves the solvothermal reactions with different amounts of VOT: (I) 50 μL, (II) 70 μL, and (III) 120 μL. The step 2 is simple annealing in air.

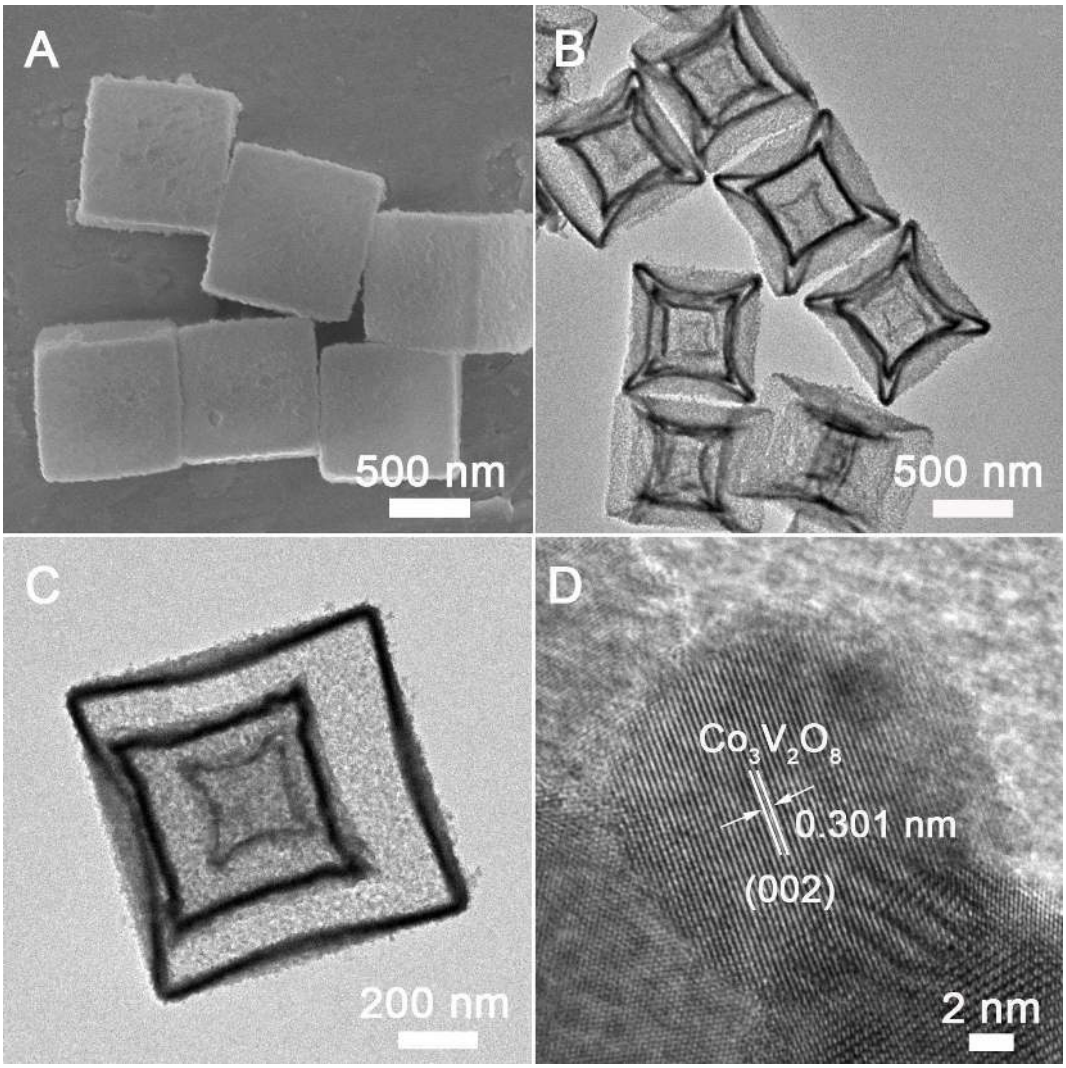

Figure 2. (A) FESEM image, (B,C) TEM images, and (D) HRTEM image of T-Co_3O_4@$Co_3V_2O_8$ nanoboxes

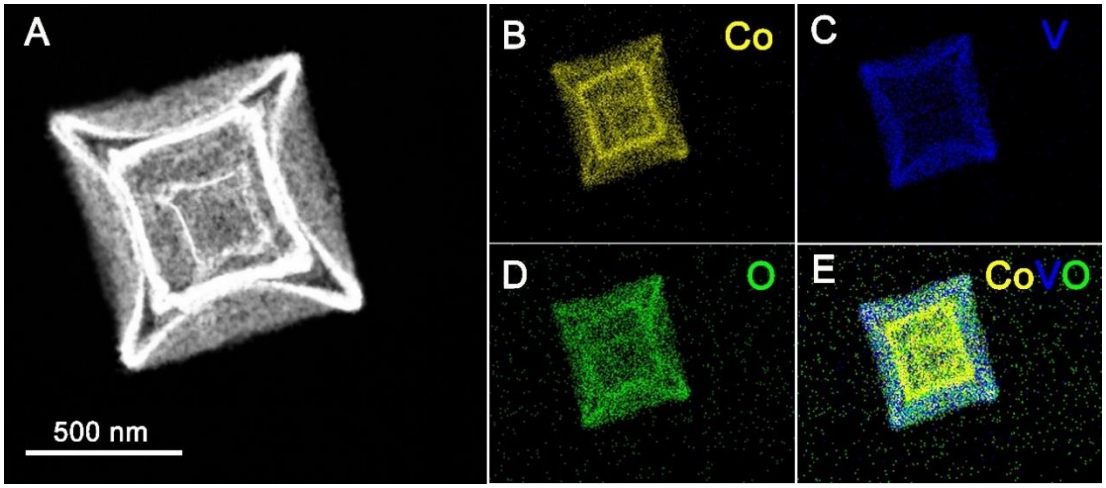

Figure 3. Elemental distributions for an individual T-Co_3O_4@$Co_3V_2O_8$ nanobox. (A) HAADF-STEM image, (B) Co mapping, (C) V mapping, (D) O mapping and (E) overlay mapping.

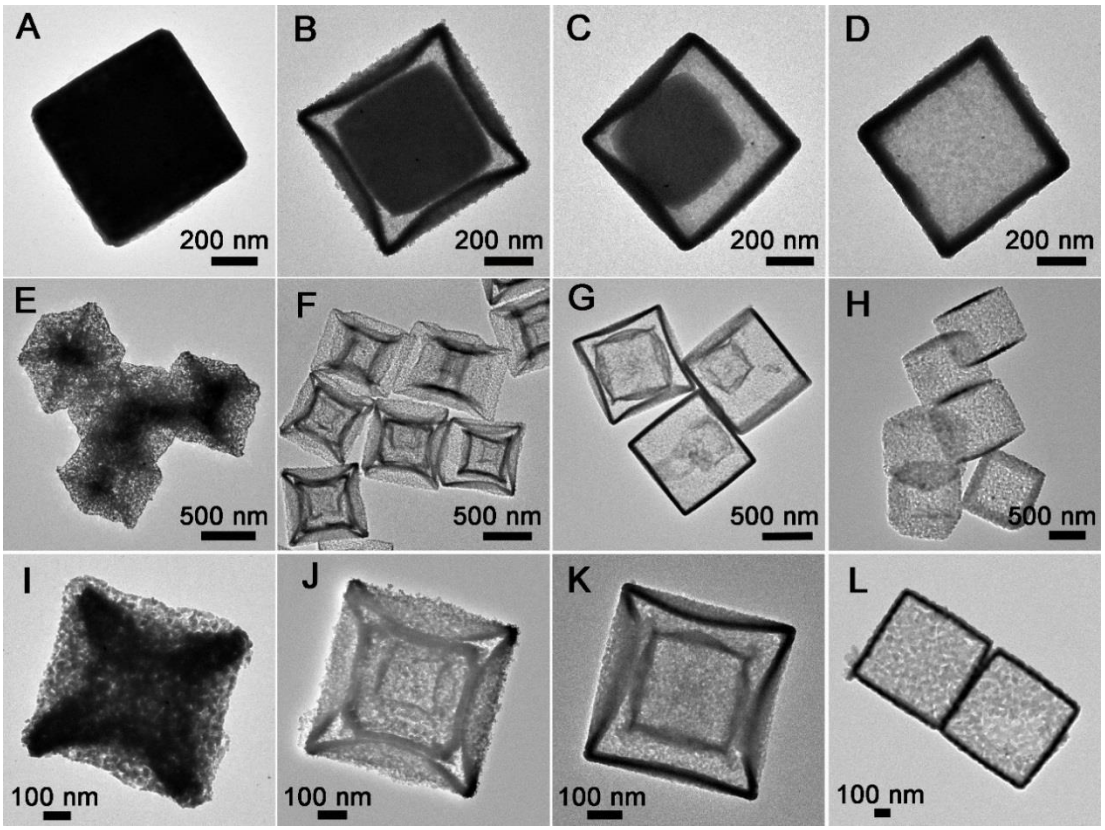

Figure 4. TEM images of the precursors prepared with different VOT concentrations (A-D) and the corresponding products after annealing in air (E-L). (A, E, I) 0 μL, (B, F, J) 50 μL, (C, G, K) 70 μL and (D, H, L) 120 μL.

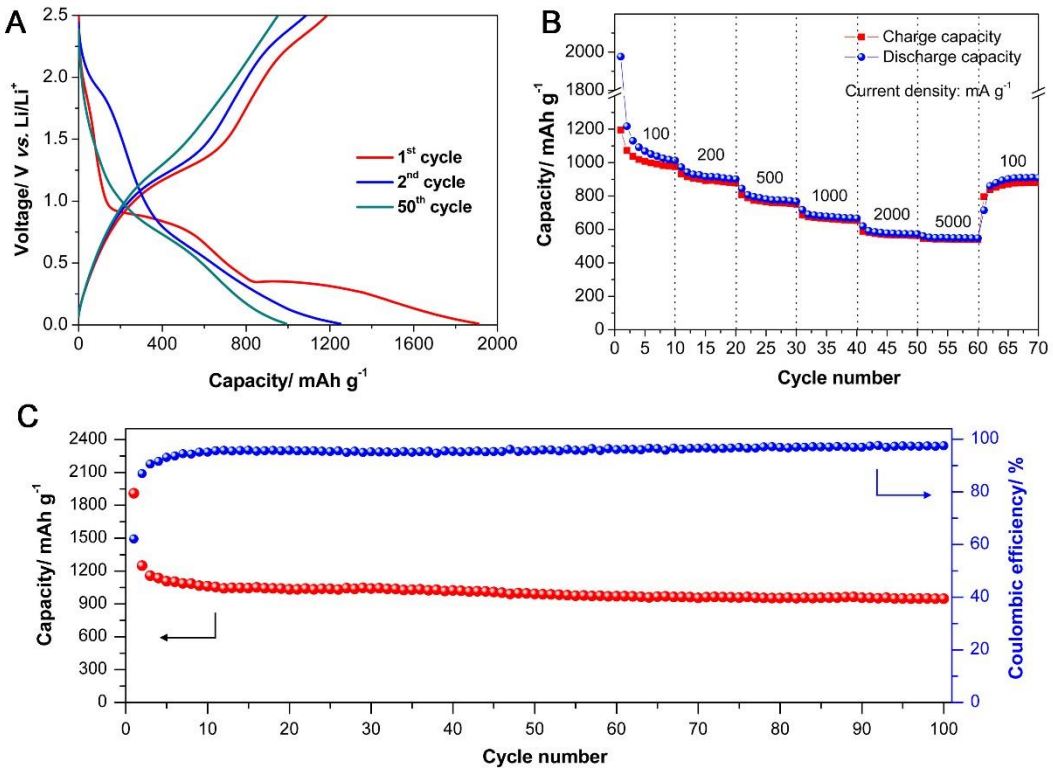

Figure 5. Electrochemical lithium storage properties of the T-Co_3O_4@$Co_3V_2O_8$ nanoboxes. (A) Charge-discharge voltage profiles at 100 mA g^{-1}, (B) rate performance, (C) cycling performance at 100 mA g^{-1} and the corresponding Coulombic efficiency.

for Table of Content Entry

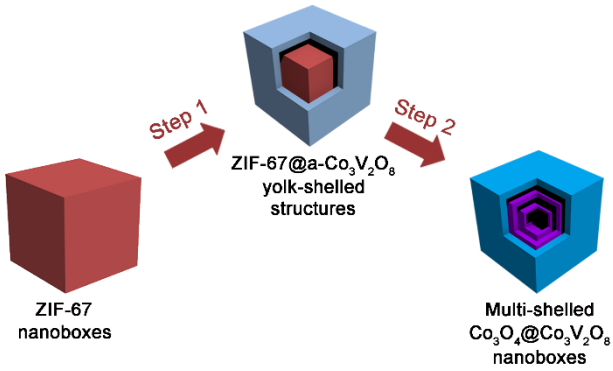

Multi-shelled Co_3O_4@$Co_3V_2O_8$ hybrid nanoboxes have been successfully synthesized via a simple metal-organic framework (MOF) engaged strategy utilizing the reaction of zeolitic imidazolate framework (ZIF)-67 with the vanadium source of vanadium oxytriisopropoxide (VOT). When evaluated as electrode materials for lithium-ion batteries, these unique nanoboxes exhibit enhanced lithium storage properties.